福島県立医科大学 学術機関リポジトリ

Title	Liver-specific G0S2 expression exacerbates hepatic insulin resistance in high fat induced insulin resistance rats(本文)
Author(s)	菅谷, 芳幸
Citation	
Issue Date	2014-03-25
URL	http://ir.fmu.ac.jp/dspace/handle/123456789/602
Rights	This is the pre-peer reviewed version of the following article: [J Diabetes. 2017 Aug;9(8):754-763], which has been published in final form at [https://doi.org/10.1111/1753-0407.12482]. This article may be used for non-commercial purposes in accordance with Wiley Terms and Conditions for Use of Self-Archived Versions.
DOI	
Text Version	ETD

This document is downloaded at: 2024-09-18T19:40:08Z

Fukushima Medical University

学　位　論　文

Liver-specific G0S2 expression exacerbates hepatic insulin resistance in high fat induced insulin-resistant rats.

(肝臓における G0S2 の過剰発現は、高脂肪餌誘発性インスリン抵抗性モデルラットにおいて肝臓でのインスリン抵抗性を増悪させる)

福島県立医科大学医学研究科

腎臓高血圧・糖尿病内分泌代謝内科講座　菅谷芳幸

ABSTRUCT

***OBJECTIVE*: Hepatic steatosis is strongly associated with insulin resistance. Recently it has been reported that G0S2 inhibited the lipolysis activity of adipose triglyceride lipase (ATGL), which is a major hepatic lipase as well as in adipocytes. Moreover, we confirmed that G0S2 protein contents were increased in the livers of high fat diet (HFD)-fed rats. However, the precise physiological role of hepatic G0S2 is still unknown.**

In the current studies, we investigated the effect of hepatic G0S2 on insulin sensitivity in normal chow diet (NCD) or HFD-fed male Wistar rats by overexpressing G0S2 protein using an adenovirus (Ad) encoding mouse G0S2.

***RESEARCH DESIGN AND METHODS*: Male Wistar rats were fed with NCD or 60% HFD for a total of 4 weeks. After 3 weeks feeding, they were injected with control Ad-GFP or Ad-G0S2. On day 7 post injection, intravenous glucose tolerance test (ivGTT) and euglycemic-hyperinsulinemic clamp studies (at 25 mU/kg/min insulin infusion rate) were performed after a 8-hour fast.**

***RESULTS*: The body weight and fasting glucose levels were not significantly different between the Ad-GFP and the Ad-G0S2 groups. In the HFD-fed rats, during the clamp studies, the glucose infusion rate (GIR) required to euglycemia was significantly decreased by 16% (from 34.9 ± 2.3 to 29.4 ± 0.8 mg/kg/min, $P < 0.05$) in the Ad-G0S2 group compared with the Ad-GFP group. Insulin-suppressed hepatic glucose output (HGO) was significantly increased from 5.1 ± 0.6 to 6.7 ± 0.5 mg/kg/min ($p < 0.05$) in the Ad-G0S2 group, but insulin-stimulated glucose disposal rate (IS-GDR) was not significantly different between two groups. On the other hand, under the NCD conditions, there were no significant changes in the GIR,**

IS-GDR, and HGO between two groups. Consistent with the clamp data, the insulin-stimulated phosphorylation of Akt (Ser473) was significantly decreased in the livers of the HFD-fed rats injected with Ad-G0S2. Furthermore, the Oil-Red O stain indicated that overexpression of G0S2 protein in liver promoted hepatic steatosis by 2.5-fold in HFD-fed rats.

***CONCLUSION*: These results indicate that hepatic G0S2 protein might promote hepatic insulin resistance by the exacerbation of hepatic steatosis.**

INTRODUCTION

Type 2 diabetes is a progressive disease, characterized by insulin resistance and impaired insulin secretion, which lead to chronic hyperglycemia and increased risk of micro- and macro-vascular complications [1]. Insulin resistance, which is characterized by an impaired ability of insulin to inhibit glucose output from the liver and to promote glucose uptake in muscle [1], is frequently well established in individuals with impaired glucose intolerance (IGT). In addition, Insulin resistance is a central component defining the metabolic syndrome, a constellation of abnormalities that include obesity, hypertension, glucose intolerance, and dyslipidemia [2].

Hepatic steatosis, defined as ectopic accumulation of triglycerides (TGs) in hepatocytes, is the first step in a spectrum of non-alcoholic fatty liver disease (NAFLD). In the two-hit model of NAFLD pathogenesis, hepatic fat accumulation is the 'first hit' and hepatic steatosis leads to 'second hit' that results in hepatocyte injury [3]. Hepatic steatosis is more frequent among people with diabetes and obesity [4, 5], and prevalence of hepatic steatosis is increasing in Japan [6]. Accumulation of TGs in the liver leads to hepatic insulin resistance [7], and moreover, hepatic steatosis is thought to be an independent determinant of cardiovascular disease [8, 9]. Hepatic steatosis develops when free fatty acid (FFA) uptake and synthesis in the liver exceeds its elimination rates [10]. A large number of molecules can be involved in the regulation of lipid metabolism in the liver.

G0/G1 switch gene 2 (G0S2) is one of the G0/G1 switch (G0S) genes that were first identified in lymphocytes during their lectin-activated switch from the G0 to the G1 phases of the cell cycle [11]. Several reports have suggested that G0S2 is a multifaceted protein with disparate functions related to proliferation, metabolism, inflammation, and

carcinogenesis. The G0S2 gene was is epigenetically silenced in head and neck cancer [12], squamous lung cancer, and cisplatin-resistant cancer cells [13]. On the other hand, the G0S2 expression was elevated in endometriosis [14], bronchial epithelial cells treated with retinoic acid [15], senescent dermal fibroblasts [16], bone marrow cells from patients with rheumatoid arthritis [17], and peripheral mononuclear cells from patients with vasculitis [18] and psoriasis [19].

G0S2 was later identified as a novel putative target gene of peroxisome proliferator-activated receptor α (PPARα) by comparing liver mRNAs of wild-type and PPARα-null mice using microarrays, and it was reported that the G0S2 mRNA level was highest in adipose tissue and was up-regulated during adipogenic differentiation of mouse 3T3-L1 cells and that G0S2 is a direct PPARs, especially PPARγ, target gene [20]. Recently, it was revealed that G0S2 inhibited adipose triglyceride lipase (ATGL) [21], which was the rate-limiting enzyme for TGs hydrolysis in adipocytes [22] and was shown to be a major hepatic lipase that regulates TGs turnover [23-25]. Hepatic expression of G0S2 was markedly increased under high sucrose diet (HSD) in Nagoya-Shibata-Yasuda (NSY) mice [26]. Wang et al. reported that Adenovirus-mediated expression of G0S2 (Ad-G0S2) potently induced hepatic steatosis in mice [27]. These studies suggest that G0S2 has an important role in regulation of hepatic TG metabolism. However, the role of G0S2 in insulin signaling is unclear. In this study, we investigated the effect of hepatic G0S2 on insulin sensitivity in normal chow diet (NCD) or high fat diet (HFD)-fed male Wistar rats by overexpressing G0S2 using Ad-G0S2.

MATERIALS AND METHODS

Materials

AdEasy™ Adenoviral Vector System was purchased from Stratagene Inc. (La Jolla, CA, USA). Adeno-X Virus Purification and Rapid Titer Kits were purchased from TAKARA BIO INC. (Shiga, JAPAN). Male Wistar rats were procured from Charles River Laboratory Japan, Inc. (Kanagawa, Japan). Insulin (Novolin R) was purchased from Novo Nordisk (Copenhagen, Denmark). High fat diet (HFD) (60% w/w, #D12492) was purchased from Research Diet Inc. (New Brunswick, NJ, USA). The catheter (Micro-Renathane MRE-033, 0.033 cm in OD and 0.014 cm in ID) was purchased from Braintree Scientific (Braintree, MA, USA). D-[3-^{3}H] glucose was purchased from PerkinElmer Inc. (Waltham, MA, USA). Pentobarbital was purchased from Kyoritsu Pharmaceutical Co. (Tokyo, Japan). The 50% dextrose was purchased from Otsuka Pharmaceutical Co. (Tokushima, Japan). BCA protein assay reagent was purchased from Thermo Fisher Scientific Inc. (Rockford, IL, USA). Complete Mini (Phosphatase and protease inhibitors) was purchased from Roche Applied Science (Mannheim, Germany). Polyvinylidine difluoride (PVDF) transfer membranes were purchased from Millipore Corp (Bedford, MA, USA). ImmunoBlock was purchased from DS Pharma Biomedical Co. Ltd (Osaka, Japan). Anti-phospho-specific Akt (Ser473), Akt, and β-actin antibodies were purchased from Cell Signaling Technology (Boston, MA, USA). G0S2 (#sc-133424) antibody and horseradish peroxidase-conjugated secondary antibody were purchased from Santa Cruz Biotechnology (Santa Cruz, CA, USA). TRIzol reagent and pCR2.1-TOPO vector were purchased from Invitrogen Life Technologies (Carlsbad, CA, USA). The RNeasy kit was

purchased from QIAGEN Inc. (Valencia, CA, USA). All other reagents were purchased from Sigma (St. Louis, MO, USA).

Subcloning of the mouse adiponectin cDNA by RT-PCR.

The mouse full-length G0S2 cDNA (312 bp) was amplified from mouse liver using the 5'-CAGATGGAAAGTGTGCAGGAGCTG-3' sense and 5'-CCGGCCTTAAG AGGCGTGCTGCCG-3' antisense primers, subcloned into the pCR2.1-TOPO (Invitrogen) and sequenced, confirming that the clones corresponded to the mouse adiponectin (GenBank(TM) accession number BC117038).

Construction of recombinant adenoviruses.

Adenovirus expressing mouse G0S2 (Ad-G0S2) was generated from the full-length cDNA, subcloned with an AdEasy™ Adenoviral Vector System (Stratagene Inc.), propagated in HEK293 cells, and purified with Adeno-X Virus Purification and Rapid Titer Kits (TAKARA BIO INC). Control Ad-GFP was isolated using the same procedure. Both recombinant viruses were dialyzed in PBS, pH 7.4, and stored in 10% glycerol/PBS at –80 °C until use.

Animal studies.

Six-week old male Wistar rats (Charles River Laboratory Japan, Inc.) were housed individually under controlled light/dark (12/12 h) and temperature conditions (25 ˚C), and had free access to water and normal chow diet (NCD) or 60% HFD (Research Diet Inc.). Rat received a fresh diet every 3 days, and food consumption rates and body weight gains were monitored every 3days. After feeding the indicated chow for 3 weeks,

the rats were implanted with 3 catheters (Micro-Renathane MRE-033, 0.033 cm in OD and 0.014 cm in ID; Braintree Scientific, Braintree, MA), as previously described [28]. In brief, 2 catheters were placed into the right jugular vein, and another one was placed into the left carotid artery under single-dose anesthesia (pentobarbital 50 mg/kg; Kyoritsu Pharmaceutical Co.) given intraperitoneally. Catheters were tunneled subcutaneously, exteriorized at the back of the neck, and filled with heparinized saline. The jugular and carotid catheters were used for infusion and blood sampling, respectively. And subsequently, they were injected intra-arterially from the catheter of the left carotid artery with 1×10^9 p.f.u. of G0S2 or GFP viruses per rat. The animals were given 7 days to fully recover from the surgery. All procedures were performed in accordance with the Guide for Care and Use of Laboratory Animals of the NIH and were approved by the Animal Subjects Committee of the Fukushima Medical University, Japan.

Glucose and insulin tolerance tests and euglycemic-hyperinsulinemic clamp procedures.

On day 7 after the adenovirus injection, glucose tolerance and insulin sensitivity was assessed using an intravenous glucose tolerance test (ivGTT) and euglycemic-hyperinsulinemic clamp. The rats were fasted for 8 hours before the start of all experiments.

For the ivGTT, the rats were injected with 0.5 g/kg body weight of dextrose (50% dextrose; Otsuka Pharmaceutical Co.) in the jugular vein. Blood samples were collected at time 0, 15, 30, 60, 90, and 120 min from the carotid artery.

The euglycemic-hyperinsulinemic clamp experiments began with a constant infusion (0.04 μCi/min) of D-[3-^{3}H] glucose (New England Nuclear). After 120 min of

tracer equilibration and basal sampling at time -10 min, and 0 min, glucose (50% dextrose, variable infusion; Otsuka Pharmaceutical Co.) and tracer (0.12 μCi/min) plus insulin (25 mU/kg/min, Novolin R; Novo Nordisk) were infused into the jugular vein as previously described [29, 30].

Small blood samples (60 μl) were drawn at 10-min intervals and immediately analyzed for glucose (Compact Electrode Blood Sugar Analyzer Antsense: HORIBA Ltd, Kyoto, Japan) to maintain the integrity of the glucose clamp throughout the duration of the experiment. Blood samples were taken at -120 min (start of experiment), -10 min and 0 min (basal), and 100 min, 110 min and 120 min (end of experiment), for determination of glucose specific activity, insulin and FFA, content. To ensure accuracy, basal and terminal sampling was performed twice, at a 10-minute interval. We confirmed that steady-state conditions were achieved at the end of the clamp before obtaining the terminal blood specimen by measuring blood glucose every ten minutes and assuring that steady state for glucose infusion and plasma glucose levels was maintained for a minimum of 20 minutes before final sampling. We define a steady-state blood glucose concentration as one where the glucose concentration and infusion rate fluctuate by 3 mg/dl or less and by 5% or less, respectively, over 10 minutes. All blood samples were immediately centrifuged, and plasma was stored at -80 ºC for subsequent analysis. After terminal blood sampling at 120 min, animals were promptly euthanized with pentobarbital (180 mg/kg). Tissues were taken and immediately frozen in liquid nitrogen and stored at -80 ºC for subsequent metabolic analysis.

Analytical procedures.

Rat insulin, human insulin, adiponectin, free fatty acid (FFA), aspartate

aminotransferase (AST), alanine aminotransferase (ALT), γ-glutamyl transpeptidase (γ-GT) were analyzed by a private laboratory (SRL Laboratory, Tokyo, Japan). Plasma glucose specific activity was measured in duplicate after zinc sulfate and barium hydroxide deproteinization.

Immunoblotting analysis.

Liver, red quadriceps muscle, and white adipose tissue used for metabolic analysis were taken from animals immediately after euthanasia, rinsed several times in cold saline to remove blood, frozen in liquid nitrogen and stored at -80 ºC. Care was taken to avoid taking sections of the liver lobes containing large blood vessels. Tissues were homogenized in liquid nitrogen and lysed in buffer containing phosphatase and protease inhibitors (Complete Mini; Roche Applied Science) according to the protocol of the manufacturer. The protein concentration was determined by BCA protein assay reagent (Thermo Fisher Scientific Inc.). Equal amounts of protein were separated by 10% sodium dodecyl sulfate-polyacrylamide gel electrophoresis (SDS-PAGE) and transferred to polyvinidene difluoride membranes (Immobilon; Millipore), and were then blocked with ImmunoBlock (DS Pharma Biomedical Co. Ltd.) overnight. The membranes were probed with primary Akt and phospho-Akt (Ser473) antibodies (Cell Signaling Technology) followed by a Horseradish peroxidase-conjugated secondary antibody (Santa Cruz Biotechnology). The immunocomplexes were visualized with ECL western blotting detection reagents (Amersham; GH Healthcare, UK). β-actin served as an internal control protein. Band intensities were quantified by densitometry using the Image-J software (NIH, Bethesda, MD, USA).

Histological examination.

A portion of liver was fixed with 10% formalin and embedded in paraffin. 3 μm sections were cut and stained with hematoxylin and eosin for examination of liver histology (BX-50, Olympus Corporation, Tokyo, Japan). The sections were also incubated with a rabbit monoclonal G0S2 antibody (Santa Cruz, CA, USA) for 12 to 16 hours at 4℃ and stained by Simple Stain MAX-PO (Nichirei Biosciences Inc., Tokyo, Japan). To examine lipid accumulation, 6 μm frozen sections were stained with Oil Red O. Ten fields in every individual section were randomly selected, and the Oil Red O-stained area and the total tissue area were measured using the Image J software. The ratio of the Oil Red O-stained area to the total tissue area was calculated (%).

Statistical analysis.

The glucose infusion rate (GIR) required to maintain euglycemia reflects the systemic insulin sensitivity. Hepatic glucose output (HGO), which reflects the hepatic insulin sensitivity, and glucose disposal rate (GDR) were calculated for the basal period and steady-state portion of the glucose clamp using the Steele equation for steady-state conditions (HGO = GDR –GIR) [31]. The insulin-stimulated GDR (IS-GDR) reflects the ability of insulin to increase GDR above the basal value, which means that IS-GDR reflects the muscle insulin sensitivity. IS-GDR is calculated by subtracting each animal's basal HGO value from the final GDR achieved at the end of the clamp period (IS-GDR = total GDR – basal HGO value).

Data are presented as mean ± SEM. Statistical differences between two groups were calculated by the unpaired Student's test. All data are distributed to ensure that the use of means and t-test is appropriate. Statistical significance was defined as $P<0.05$.

RESULTS

G0S2 protein levels in liver, muscle, and white adipose tissues in the basal state.

We first investigated the expression of G0S2 protein in the liver, skeletal muscle and white adipose tissues of control rats by western blot analysis. In liver and white adipose tissues, G0S2 protein levels of HFD-fed rats were significantly higher than those of NCD-fed rats (Figure 1A and 1C). However, the G0S2 protein level in skeletal muscles were no significant changes in NCD- and HFD-fed rats (Figure 1B).

To confirm the G0S2 protein expression by Ad-G0S2, we performed western blotting of cell lysates obtained from either Ad-G0S2- or Ad-GFP- infected HEK 293 cells. The expression of G0S2 protein was detected in cells infected with Ad-G0S2, but did not detected in cells infected with Ad-GFP (Figure 1C).

Representative results of immunohistochemistry of G0S2 proteins in livers of rats infected with Ad-G0S2 or Ad-GFP are shown in Figure 4E. Staining for G0S2 proteins was localized to the cytoplasm of hepatocytes. G0S2 protein levels were higher in the liver tissues infected with Ad-G0S2 than with Ad-GFP. G0S2 proteins levels of Ad-G0S2-infected liver tissues were determined by western blot analysis (Figure 1F).

Overall animal characteristics.

Table 1 shows some of the general characteristics of the rats in the basal state on day 7 after injection of Ad-G0S2 or control Ad-GFP under the NCD or HFD conditions. The body weight, liver weight, and food intakes (data not shown) were not different between the Ad-G0S2 and control Ad-GFP groups, while the body weight and liver weight of the HFD-fed rats were significantly greater than those of the NCD-fed rats. There were no significant differences in glucose, insulin, and HOMA-IR levels between

the Ad-G0S2-infected rats and the Ad-GFP-infected rats, although those levels of the HFD-fed rats tended to be higher than that of NCD-fed rats. Adiponectin, FFA, AST, ALT, and γ-GTT levels did not differ significantly between two groups.

NCD-feeding studies.

Intravenous glucose tolerance tests.

On 7 days after injection of adenoviruses, ivGTTs were performed on 8-h-fasted rats. 0.5 g/kg glucose was injected into the jugular vein. There were no obvious differences in glucose levels between the Ad-G0S2-infected rats and the Ad-GFP-infected rats under the NCD conditions (Figure 2A). It was the same result for insulin levels (Figure 2B).

Euglycemic-hyperinsulinemic clamps.

To directly examine the metabolic impact of G0S2 protein on insulin sensitivity, we next subjected both groups of rats to euglycemic-hyperinsulinemic clamps at maximal (25 mU/kg/min) insulin infusion rate. Steady-state glucose and insulin levels during the clamp studies were similar in the two groups (Table 1). During these studies, we measured insulin stimulation of whole-body GDR and suppression of HGO. The GIR required to maintain euglycemia didn't differ between the two groups (Figure 3A). To assess the insulin-stimulated component of glucose disposal, the IS-GDR was calculated. The IS-GDR didn't differ between the two groups, either (Figure 3B).

Basal HGO values were not different between the Ad-G0S2-infected rats and the Ad-GFP-infected rats. During the clamp studies, HGO values didn't differ between the two groups, either (Figure 3C).

HFD-feeding studies.

Intravenous glucose tolerance tests.

Fasting glucose and insulin levels showed no significant differences between the Ad-G0S2-infected rats and the Ad-GFP-infected rats under the HFD conditions (Figure 4A, 4B). However, after the 0.5 g/kg glucose load, the glucose levels were significantly higher in the Ad-G0S2-infected rats at 15 and 30 min (283.3 ± 11.4 vs. 244.9 ± 10.7 mg/dl and 226.2 ± 9.4 vs. 195.9 ± 8.7 mg/dl respectively, $p < 0.05$) (Figure 4A). Contrary to our expectation, there were no significant differences in insulin levels during ivGTT studies between the two groups (Figure 4B).

Euglycemic-hyperinsulinemic clamps.

Steady-state glucose and insulin levels during the clamp studies were similar in the two groups (Table 1). The GIR required to maintain euglycemia was significantly decreased by 16% (from 34.9 ± 2.3 to 29.4 ± 0.8 mg/kg/min, $P < 0.05$) in the Ad-G0S2-infected rats, showing impaired overall insulin sensitivity (Figure 5A). The IS-GDR didn't differ between the two groups (Figure 5B).

Basal HGO values were not different between the Ad-G0S2-infected rats and the Ad-GFP-infected rats (9.9 ± 0.6 and 9.5 ± 0.6 mg/kg/min) (Figure 5C). During the clamp studies, HGO values were significantly higher in the Ad-G0S2-infected rats than in the Ad-AGF-infected rats (6.7 ± 0.5 vs. 5.1 ± 0.6 mg/kg/min, $P < 0.05$) (Figure 3C), suggesting that the G0S2 protein promotes hepatic insulin resistance.

Insulin signaling studies.

To assess the potential cellular mechanisms of G0S2-induced impairment in insulin sensitivity, we obtained liver, skeletal muscle and white adipose tissue samples

from the rats at the end of the euglycemic-hyperinsulinemic clamp. These samples, which represent the fully insulinized state at the termination of the glucose clamp study, were homogenized and the protein lysates were subjected to immunoblotting.

We measured Akt phosphorylation (Ser473), which is the most important molecule of the insulin signaling. Insulin led to a marked stimulation of Akt phosphorylation in liver, skeletal muscle, and white adipose tissues from control basal state rats under the NCD conditions (Figure 6A, 6B, and 6C). There were no significant differences in Akt phosphorylation between the Ad-G0S2-infected rats and the Ad-GFP-infected rats in liver, muscle, and white adipose tissues. On the other hand, this effect of Akt phosphorylation at Ser437 was significantly decreased by 65% ($P < 0.05$) in livers under the HFD conditions (Figure 7A), but not in muscle and white adipose tissues of the Ad-G0S2-infected rats (Figure 7B, 7C).

Histological examination.

Macroscopically, the livers we harvested from the Ad-G0S2-infected rats and the Ad-GFP-infected rats looked the same, although livers of the HFD-fed rats looked fattier than those of the NCD-fed rats (Figure 8A). To evaluate lipid accumulation, the livers were subsequently sectioned and stained with Oil Red O, which stains neutral lipids (Figure 8B). Oil Red O staining areas of the HFD-fed rats were significantly larger than those of NCD-fed rats. This increase of lipid accumulation was augmented by 2.5-fold in the G0S2-infected rats under the HFD conditions, but not under the NCD conditions. This result suggests hepatic insulin resistance is worsen in the Ad-G0S2-infected rats under the HFD conditions, and supports the results of ivGTT, euglycemic hyperinsulinemic clamp, and western blotting studies.

DISCUSSION

Results from the present study demonstrated that under HDF condition, not under NCD condition, G0S2 induced the lipid accumulation in the rat liver and developed hepatic steatosis. G0S2 overexpression impaired the total insulin sensitivity by promoting the hepatic insulin resistance. These findings suggest that G0S2 is an important regulator of hepatic glycolipid metabolism.

The liver is one of the primary organs responsible for controlling energy homeostasis in mammals. Hepatic steatosis arises from an imbalance between TG acquisition and removal. The fatty acids used for hepatic TG formation are derived from diet, de novo synthesis, and adipose tissue. Dietary fats taken up in the intestine are packaged into TG-rich chylomicron and delivered to the systemic circulation, and ~20% of the TG in chylomicron is delivered to the liver [32]. Carbohydrate feeding promotes de novo synthesis of FFA from acetyl-coenzyme A (CoA) by increasing the level of insulin and the availability of substrate. Insulin stimulates the transcription factor sterol regulatory element-binding protein-1c (SREBP-1c) via a signaling cascade involving Akt2, LXR, and mTOR [33]. SREBP-1c up-regulates the enzymes that catalyze lipogenesis [34]. Glucose also promotes lipogenesis by activating the transcription factor carbohydrate responsive element-binding protein (ChREBP) [35]. During fasting, plasma levels of insulin fall, whereas levels of glucagon and epinephrine increase, stimulating TG hydrolysis in adipocytes. The first step in TG hydrolysis is catalyzed by ATGL that is the rate-limiting enzyme [22].

ATGL is expressed at lower levels in non-adipose tissues such as heart, muscle, and liver [36]. In most tissues of ATGL null mice, the ectopic lipid accumulation was increased (21-fold in cardiac muscle, 3-fold in skeletal muscle, and 2.3-fold in liver) [37].

Adenovirus-mediated knockdown of ATGL reportedly developed hepatic steatosis in mice [23]. On the other hand, it was reported that adenovirus-mediated overexpression of ATGL decreased hepatic steatosis in HFD-fed mice [24]. Liver-specific ATGL knockout mice were shown to have severe progressive periportal macrovesicular and pericentral macrovesicular hepatic steatosis [25]. These studies suggest that ATGL is a major hepatic lipase that regulates TG turnover.

ATGL activity is strongly influenced by regulatory proteins. Lass et al. identified comparative gene identification-58 (CGI-58) as coactivator of ATGL, which is required for efficient lipolysis [38]. CGI-58 null mice increased fat mass and die a few hours after birth, most likely due to a severe skin defect. These studies suggest that CGI-58 is essential for ATGL activation [39]. On the other hand, more recently, Yang et al. identified G0S2, which had been first identified as a potential cell cycle regulator [11], as an inhibitory protein of ATGL [21].

When overexpressed in HeLa cells, G0S2 localized to lipid droplets and prevented ATGL-mediated TG hydrolysis by binding to ATGL [21]. Although G0S2 is mainly expressed in brown and white adipose tissue, G0S2 mRNA is reasonably well expressed in other tissues, such as lung, liver, and heart. [20]. Hepatic expression of G0S2 was markedly increased in only HSD-fed NSY mice, not in HSD-fed C3H mice, while HSD developed hepatic steatosis and promoted insulin resistance [26]. We reported here that Ad-G0S2-infected rats, only under HFD conditions, developed hepatic steatosis and promoted insulin resistance. Hepatic expression of G0S2 was up-regulated by fasting and by PPARα agonist while G0S2 expression was up-regulated during the adipogenesis of mouse 3T3-L1 cells [20]. Recently, Wang et al. reported that Adenovirus-mediated expression of G0S2 potently induced hepatic steatosis in mice, and G0S2 was found to be

co-localized with ATGL at the surface of lipid droplets [27]. In this study here, consistent with observations of Wang et al., the Ad-G0S2-infected rats developed hepatic steatosis under HFD conditions, although this effect wasn't observed under NCD conditions. This effect of lipid accumulation in liver might be due to G0S2 inhibiting AGTL activity.

A number of studies have reported a strong relationship between hepatic steatosis and insulin resistance [5, 7, 40-43]. Fat accumulation in the liver is associated with defects in insulin suppression of HGO independent of obesity[44, 45]. Hepatic insulin resistance can occur independently of changes in circulating adipocytokines such as tumor necrosis factor-α (TNF-α), interleukin-6 (IL-6), resistin, adiponectin, and retinol binding protein-4 (RBP-4) [43]. Hepatic resistance was associated with an increase in hepatic diglyceride (DG) content [41]. The link between hepatic DAG accumulation and hepatic insulin resistance could be attributed to activation of protein kinase Cε (PKCε) [46], which was predominant PKC isoforms activated in liver following fat feeding [7]. The mechanism for lipid-induced insulin resistance is similar to what is observed in skeletal muscle where PKCθ has been shown to be the predominant novel PKC isoform activated during lipid-induced muscle insulin resistance [47, 48]. Activated by DG, PKCε inhibits the insulin receptor kinase. This then leads to decreased insulin-stimulated tyrosine phosphorylation of insulin receptor substrate 1 and 2 (IRS1, IRS2), resulting in reduced insulin activation of 1-phosphoinositol 3-kinase (PI 3-kinase), and Akt2. Reduced Akt2 activation results in decreased glycogen synthase (GS)-mediated glycogen synthesis and decreased suppression of gluconeogenesis, which in turn leads to glucose release through glucose transporter 2 (GLUT2).

Considering that G0S2 inhibits ATGL activity, inactivation of ATGL might be involved in modifying insulin resistance in the Ad-G0S2-infected rats. However, the

association between ATGL and insulin resistance is controversial. Haemmerle et al. reported that glucose and insulin tolerances were improved in ATGL-KO mice under NCD conditions [37]. Wu et al. reported that there were no differences in liver-specific ATGL-KO mice under both NCD and HFD conditions during GTT and ITT [25]. On the other hand, Ong et al. reported that adenovirus-mediated overexpression of ATGL improved insulin tolerance under NCD conditions [24]. With regard to G0S2, Wang et al. reported that, during oral GTT, G0S2 overexpression in the liver significantly improved glucose tolerance in mice under standard rodent chow conditions, whereas there were no significant differences in glucose levels during insulin tolerance test [27]. In these studies, DG content in the liver wasn't assessed, and most studies were investigated under only NCD conditions. They assessed insulin resistance by GTT or ITT. These methods are indirect for quantifying insulin sensitivity. In the present study, we used euglycemic-hyperinsulinemic clamp, which is the gold standard for quantifying hepatic insulin sensitivity. We found that the Ad-G0S2-infected rats promoted hepatic insulin resistance under HFD conditions, which was consistent with the results of IV-GTT and Western blotting analysis in this study. Fed with HFD, the amount of TGs, which are derived from chylomicron, is increased in liver with the result of growing lipid droplets. In the Ad-G0S2 infected rats, under HDF conditions, G0S2 inhibits ATGL-mediated TG hydrolysis in droplets and TG content is increased. At the same time, in the endoplasmic reticulum (ER), TGs are also synthesized from DGs, which is a part of de novo lipogenesis [49]. The synthesis of TGs from DGs is catalyzed by acyl CoA: diacylglycerol acyltransferase (DGAT) enzymes. Wu et al. reported that DGAT2 mRNA was markedly decreased in liver-specific ATGL-KO mice [25], which indicates that TG synthesis might be down-regulated by some kind of negative feedback mechanism. Then,

DG content might be increased in liver and promote hepatic insulin resistance. However, DG content in liver is yet to be assessed, and the detail mechanisms of promoting hepatic insulin resistance by G0S2 still remain to be elucidated.

In conclusion, G0S2 might promote hepatic insulin resistance by the exacerbation of hepatic steatosis under HFD conditions. The further investigations are needed to reveal the mechanism of G0S2 for insulin sensitivity.

ACKNOWLEDHMENTS

I thanked Tsuyoshi Watanabe MD, PhD and Hiroaki Satoh MD, PhD for expert assistance, Yuko Ohashi and Atsuko Hashimoto for excellent technical assistance.

REFERENCES

1. Olefsky, J.M. and C.K. Glass, *Macrophages, inflammation, and insulin resistance.* Annu Rev Physiol, 2010. **72**: p. 219-46.
2. Flier, J.S., *Obesity wars: molecular progress confronts an expanding epidemic.* Cell, 2004. **116**(2): p. 337-50.
3. Day, C.P. and O.F. James, *Steatohepatitis: a tale of two "hits"?* Gastroenterology, 1998. **114**(4): p. 842-5.
4. Adams, L.A., P. Angulo, and K.D. Lindor, *Nonalcoholic fatty liver disease.* CMAJ, 2005. **172**(7): p. 899-905.
5. Richard, J. and I. Lingvay, *Hepatic steatosis and Type 2 diabetes: current and future treatment considerations.* Expert Rev Cardiovasc Ther, 2011. **9**(3): p. 321-8.
6. Kojima, S., et al., *Increase in the prevalence of fatty liver in Japan over the past 12 years: analysis of clinical background.* J Gastroenterol, 2003. **38**(10): p. 954-61.
7. Samuel, V.T., et al., *Mechanism of hepatic insulin resistance in non-alcoholic fatty liver disease.* J Biol Chem, 2004. **279**(31): p. 32345-53.
8. Targher, G., et al., *Relation of nonalcoholic hepatic steatosis to early carotid atherosclerosis in healthy men: role of visceral fat accumulation.* Diabetes Care, 2004. **27**(10): p. 2498-500.
9. Targher, G., C.P. Day, and E. Bonora, *Risk of cardiovascular disease in patients with nonalcoholic fatty liver disease.* N Engl J Med, 2010. **363**(14): p. 1341-50.
10. De Bruyne, R.M., E. Fitzpatrick, and A. Dhawan, *Fatty liver disease in children: eat now pay later.* Hepatol Int, 2010. **4**(1): p. 375-85.
11. Russell, L. and D.R. Forsdyke, *A human putative lymphocyte G0/G1 switch gene containing a CpG-rich island encodes a small basic protein with the potential to be phosphorylated.* DNA Cell Biol, 1991. **10**(8): p. 581-91.
12. Tokumaru, Y., et al., *Inverse correlation between cyclin A1 hypermethylation and p53 mutation in head and neck cancer identified*

by reversal of epigenetic silencing. Cancer Res, 2004. **64**(17): p. 5982-7.

13. Kusakabe, M., et al., *Impact of DNA demethylation of the G0S2 gene on the transcription of G0S2 in squamous lung cancer cell lines with or without nuclear receptor agonists.* Biochem Biophys Res Commun, 2009. **390**(4): p. 1283-7.
14. Kao, L.C., et al., *Expression profiling of endometrium from women with endometriosis reveals candidate genes for disease-based implantation failure and infertility.* Endocrinology, 2003. **144**(7): p. 2870-81.
15. Ma, Y., et al., *Microarray analysis uncovers retinoid targets in human bronchial epithelial cells.* Oncogene, 2003. **22**(31): p. 4924-32.
16. Yoon, I.K., et al., *Exploration of replicative senescence-associated genes in human dermal fibroblasts by cDNA microarray technology.* Exp Gerontol, 2004. **39**(9): p. 1369-78.
17. Nakamura, N., et al., *Isolation and expression profiling of genes upregulated in bone marrow-derived mononuclear cells of rheumatoid arthritis patients.* DNA Res, 2006. **13**(4): p. 169-83.
18. Kobayashi, S., et al., *Expression profiling of PBMC-based diagnostic gene markers isolated from vasculitis patients.* DNA Res, 2008. **15**(4): p. 253-65.
19. Koczan, D., et al., *Gene expression profiling of peripheral blood mononuclear leukocytes from psoriasis patients identifies new immune regulatory molecules.* Eur J Dermatol, 2005. **15**(4): p. 251-7.
20. Zandbergen, F., et al., *The G0/G1 switch gene 2 is a novel PPAR target gene.* Biochem J, 2005. **392**(Pt 2): p. 313-24.
21. Yang, X., et al., *The G(0)/G(1) switch gene 2 regulates adipose lipolysis through association with adipose triglyceride lipase.* Cell Metab, 2010. **11**(3): p. 194-205.
22. Zimmermann, R., et al., *Fat mobilization in adipose tissue is promoted by adipose triglyceride lipase.* Science, 2004. **306**(5700):

p. 1383-6.

23. Ong, K.T., et al., *Adipose triglyceride lipase is a major hepatic lipase that regulates triacylglycerol turnover and fatty acid signaling and partitioning.* Hepatology, 2011. **53**(1): p. 116-26.
24. Turpin, S.M., et al., *Adipose triacylglycerol lipase is a major regulator of hepatic lipid metabolism but not insulin sensitivity in mice.* Diabetologia, 2011. **54**(1): p. 146-56.
25. Wu, J.W., et al., *Deficiency of liver adipose triglyceride lipase in mice causes progressive hepatic steatosis.* Hepatology, 2011. **54**(1): p. 122-32.
26. Nojima, K., et al., *Analysis of hepatic gene expression profile in a spontaneous mouse model of type 2 diabetes under a high sucrose diet.* Endocr J, 2013. **60**(3): p. 261-74.
27. Wang, Y., et al., *The g0/g1 switch gene 2 is an important regulator of hepatic triglyceride metabolism.* PLoS One, 2013. **8**(8): p. e72315.
28. Hirai, H., et al., *Interaction between resistin and adiponectin in the proliferation of rat vascular smooth muscle cells.* Mol Cell Endocrinol, 2013. **366**(1): p. 108-16.
29. Satoh, H., et al., *Adenovirus-mediated chronic "hyper-resistinemia" leads to in vivo insulin resistance in normal rats.* J Clin Invest, 2004. **114**(2): p. 224-31.
30. Satoh, H., et al., *Adenovirus-mediated adiponectin expression augments skeletal muscle insulin sensitivity in male Wistar rats.* Diabetes, 2005. **54**(5): p. 1304-13.
31. Steele, R., *Influences of glucose loading and of injected insulin on hepatic glucose output.* Ann N Y Acad Sci, 1959. **82**: p. 420-30.
32. Redgrave, T.G., *Formation of cholesteryl ester-rich particulate lipid during metabolism of chylomicrons.* J Clin Invest, 1970. **49**(3): p. 465-71.
33. Li, S., M.S. Brown, and J.L. Goldstein, *Bifurcation of insulin signaling pathway in rat liver: mTORC1 required for stimulation of lipogenesis, but not inhibition of gluconeogenesis.* Proc Natl Acad

Sci U S A, 2010. **107**(8): p. 3441-6.

34. Horton, J.D., J.L. Goldstein, and M.S. Brown, *SREBPs: activators of the complete program of cholesterol and fatty acid synthesis in the liver.* Journal of Clinical Investigation, 2002. **109**(9): p. 1125-1131.
35. Uyeda, K. and J.J. Repa, *Carbohydrate response element binding protein, ChREBP, a transcription factor coupling hepatic glucose utilization and lipid synthesis.* Cell Metab, 2006. **4**(2): p. 107-10.
36. Kershaw, E.E., et al., *Adipose triglyceride lipase: function, regulation by insulin, and comparison with adiponutrin.* Diabetes, 2006. **55**(1): p. 148-57.
37. Haemmerle, G., et al., *Defective lipolysis and altered energy metabolism in mice lacking adipose triglyceride lipase.* Science, 2006. **312**(5774): p. 734-7.
38. Lass, A., et al., *Adipose triglyceride lipase-mediated lipolysis of cellular fat stores is activated by CGI-58 and defective in Chanarin-Dorfman Syndrome.* Cell Metab, 2006. **3**(5): p. 309-19.
39. Radner, F.P., et al., *Growth retardation, impaired triacylglycerol catabolism, hepatic steatosis, and lethal skin barrier defect in mice lacking comparative gene identification-58 (CGI-58).* J Biol Chem, 2010. **285**(10): p. 7300-11.
40. Cohen, J.C., J.D. Horton, and H.H. Hobbs, *Human fatty liver disease: old questions and new insights.* Science, 2011. **332**(6037): p. 1519-23.
41. Jornayvaz, F.R. and G.I. Shulman, *Diacylglycerol activation of protein kinase Cepsilon and hepatic insulin resistance.* Cell Metab, 2012. **15**(5): p. 574-84.
42. Fabbrini, E., et al., *Alterations in adipose tissue and hepatic lipid kinetics in obese men and women with nonalcoholic fatty liver disease.* Gastroenterology, 2008. **134**(2): p. 424-31.
43. Kim, J.K., et al., *Tissue-specific overexpression of lipoprotein lipase causes tissue-specific insulin resistance.* Proc Natl Acad Sci U S A, 2001. **98**(13): p. 7522-7.

44. Seppala-Lindroos, A., et al., *Fat accumulation in the liver is associated with defects in insulin suppression of glucose production and serum free fatty acids independent of obesity in normal men.* J Clin Endocrinol Metab, 2002. **87**(7): p. 3023-8.
45. Bugianesi, E., et al., *Insulin resistance in non-diabetic patients with non-alcoholic fatty liver disease: sites and mechanisms.* Diabetologia, 2005. **48**(4): p. 634-42.
46. Farese, R.V., *Phospholipid signaling systems in insulin action.* Am J Med, 1988. **85**(5a): p. 36-43.
47. Griffin, M.E., et al., *Free fatty acid-induced insulin resistance is associated with activation of protein kinase C theta and alterations in the insulin signaling cascade.* Diabetes, 1999. **48**(6): p. 1270-4.
48. Yu, C., et al., *Mechanism by which fatty acids inhibit insulin activation of insulin receptor substrate-1 (IRS-1)-associated phosphatidylinositol 3-kinase activity in muscle.* J Biol Chem, 2002. **277**(52): p. 50230-6.
49. Yen, C.L., et al., *Thematic review series: glycerolipids. DGAT enzymes and triacylglycerol biosynthesis.* J Lipid Res, 2008. **49**(11): p. 2283-301.

FIGURE LEGENDS

Figure 1. Expression of G0S2 in each tissues of male Wistar rats, and overexpression of G0S2 in HEK293 cells and livers of male Wister rats.

Six week-old male Wistar rats were fed with NCD (open bar) or HFD (closed bar) for 4 weeks. G0S2 protein levels in the liver (A), skeletal muscle (B), and WAT (C) were determined with western blotting. (D) G0S2 or GFP proteins levels in HEK293 cells, which were infected with Ad-G0S2 or Ad-GFP for 48 hours respectively, were also determined. (E) Immunological detection of G0S2 proteins in livers of male Wistar rats. (F) G0S2 protein levels in livers of Ad-GFP or Ad-G0S2-infected rats were determined with western blotting. Values are means ± SE (n = 4). *$P < 0.05$ vs. NCD-fed rats.

Figure 2. IV-GTT in NCD-fed rats on postinjection day 7.

Glucose (A) and insulin (B) curves from the GTT in Ad-GFP (open circle, n = 7) and Ad-G0S2 (closed circle, n = 7)-infected rats injected with 0.5 g/kg body weight after 8-h fast. Values are means± SE.

Figure 3. Euglycemic hyperinsulinemic clamp in NCD-fed rats on postinjection day7.

GIR (A), IS-GDR (B), and in Ad-GFP (open bar, n = 10) and Ad-G0S2 (closed bar, n = 10)-infected rats after 8-h fast. HGO (C) was calculated at the basal state (open bar) and during clamp (closed bar). Insulin infusion rates were 25 mU/kg/min. Values are means± SE. †$P < 0.05$, ††$P < 0.01$ vs. basal state.

Figure 4. IV-GTT in HFD-fed rats on postinjection day 7.

Glucose (A) and insulin (B) curves from the GTT in Ad-GFP (open circle, n = 7) and Ad-G0S2 (closed circle, n = 9)-infected rats injected with 0.5 g/kg body weight after 8-h fast. Values are means± SE. *$P < 0.05$ vs. Ad-GFP-infected rats.

Figure 5. Euglycemic hyperinsulinemic clamp in HFD-fed rats on postinjection day 7.

GIR (A), IS-GDR (B), and in Ad-GFP (open bar, n = 8) and Ad-G0S2 (closed bar, n = 10)-infected rats after 8-h fast. HGO (C) was calculated at the basal state (open bar) and during clamp (closed bar). Insulin infusion rates were 25 mU/kg/min. Values are means± SE. *$P < 0.05$ vs. Ad-GFP-infected rats; †$P < 0.05$, ††$P < 0.01$ vs. basal state.

Figure 6. Effect of G0S2 protein on Akt phosphorylation (Ser473) in each tissues of NCD-fed rats on postinjection day 7.

Akt and pAkt (Ser473) protein levels in the liver (A), skeletal muscle (B), and WAT (C) of Ad-GFP (open bar) and Ad-G0S2 (closed bar)-infected rats were determined with western blotting. Values are means± SE (n = 4). †$P < 0.05$, ††$P < 0.01$ vs. basal state.

Figure 7. Effect of G0S2 protein on Akt phosphorylation (Ser473) in each tissues of HFD-fed rats on postinjection day 7.

Akt and pAkt (Ser473) protein levels in the liver (A), skeletal muscle (B), and WAT (C) of Ad-GFP (open bar) and Ad-G0S2 (closed bar)-infected rats were determined with western blotting. Values are means± SE (n = 4). *$P < 0.05$ vs. Ad-GFP-infected rats; †$P < 0.05$ vs. basal state.

Figure 8. Macroscopic and microscopic aspect of livers postinjection day 7.

(A) Photographs of livers at macroscopic scale. (B) The liver sections were stained with Oil Red O (x400). (C) The ratio of the Oil Red O-stained area to the total tissue area was calculated (%) (open bar for Ad-GFP-infected rats, closed bar for Ad-G0S2 infected rats). Values are means± SE (n = 6). $^{**}P < 0.01$vs. Ad-GFP-infected rats; †$P < 0.05$ vs. NCD-fed rats.

Table 1

Plasma measurements in the basal state and euglycemic-hyperinsulinemic clamps

	Ad-GFP (n)	Ad-G0S2 (n)
Body weight [g]	408.4 ± 8.5(21)	407.8 ± 6.1 (24)
Liver weight [g]	14.3 ± 0.5 (6)	14.7 ± 0.7 (6)
Basal		
Glucose [mg/dL]	178.1 ± 7.8 (13)	180.7 ± 6.8 (16)
Insulin [ng/mL]	4.48 ± 0.32 (13)	4.75 ± 0.76 (16)
HOMA-IR	2.01 ± 0.23 (13)	2.09 ± 0.48 (16)
Glucagon [pg/mL]	57.3 ± 5.2 (6)	73.5 ± 4.7 (6) *
Adiponectin [μg/mL]	1.42 ± 0.10 (6)	1.35 ± 0.07 (6)
FFA [μEQ/L]	262.7 ± 42.2 (6)	270.8 ± 42.0 (6)
TG [mg/dL]	56.0 ± 10.3 (6)	59.7 ± 10.2 (6)
TC [mg/dL]	63.2 ± 5.8 (6)	57.1 ± 5.9 (6)
HDL-C [mg/dL]	18.7 ± 1.0 (6)	17.3 ± 1.4 (6)
Liver function		
AST [IU/L]	81.7 ± 10.9(6)	60.8 ± 4.6(6)
ALT [IU/L]	26.5 ± 1.7(6)	28.3 ± 1.6(6)
γ-GTT [IU/L]	3.0 ± 0.0(6)	3.0 ± 0.0(6)
Clamp		
Glucose [mg/dl]	146.9 ±1.7 (8)	149.8 ± 1.1 (10)
Human insulin [μIU/mL]	1039.7 ± 87.5 (6)	1260.0 ± 63.9 (6)
FFA [μEQ/L]	63.8 ± 13.4 (6)	55.7 ± 17.9 (6)
Suppression rate [%]	75.7	79.4

Values are means± SE. *$P < 0.01$vs. Ad-GFP-infected rats

Figure 1.

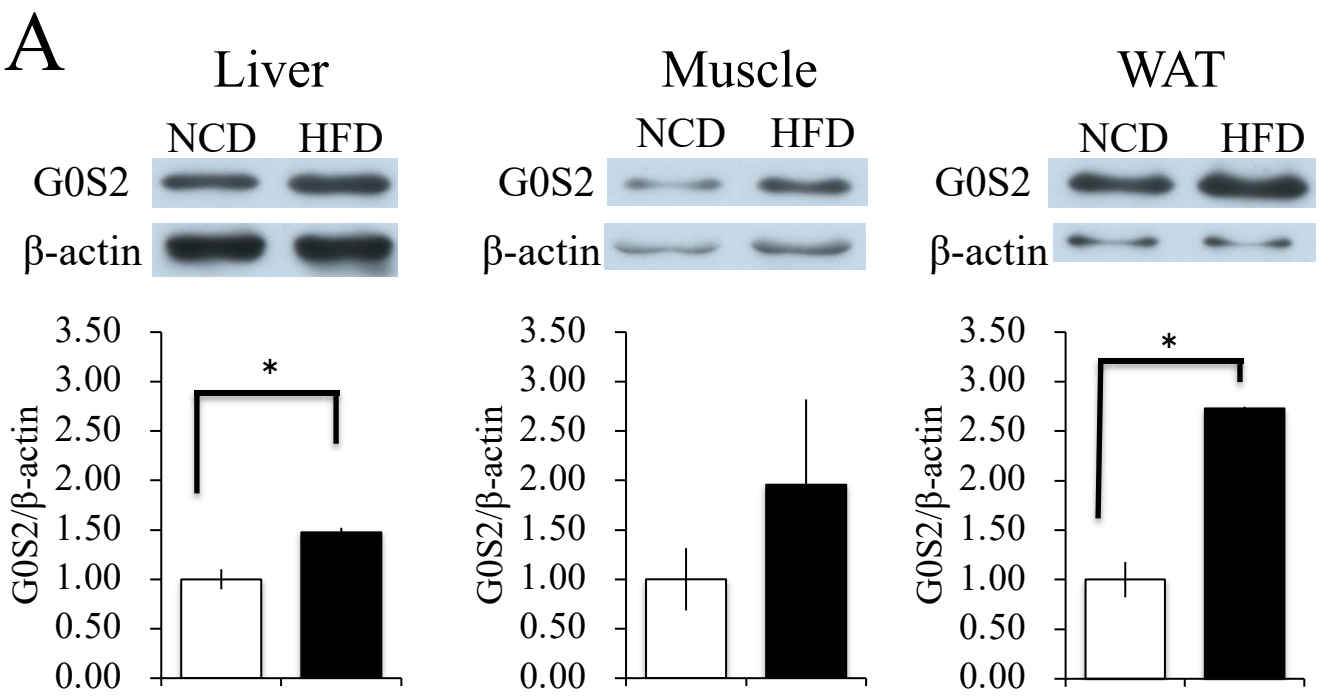
A
Liver
Muscle
WAT
NCD
HFD
G0S2
β-actin
G0S2/β-actin
3.50
3.00
2.50
2.00
1.50
1.00
0.50
0.00
*

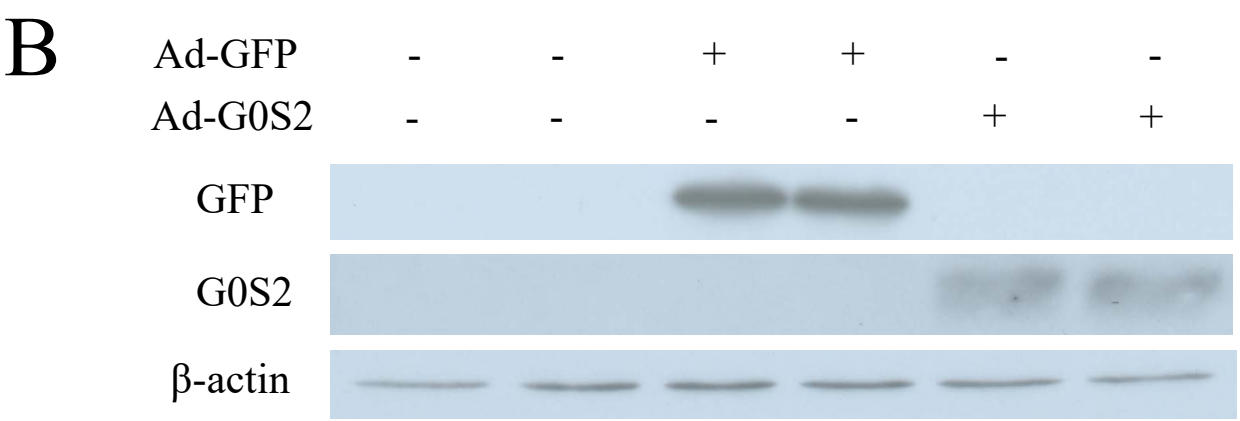
B
Ad-GFP
Ad-G0S2
GFP
G0S2
β-actin

Figure 2.

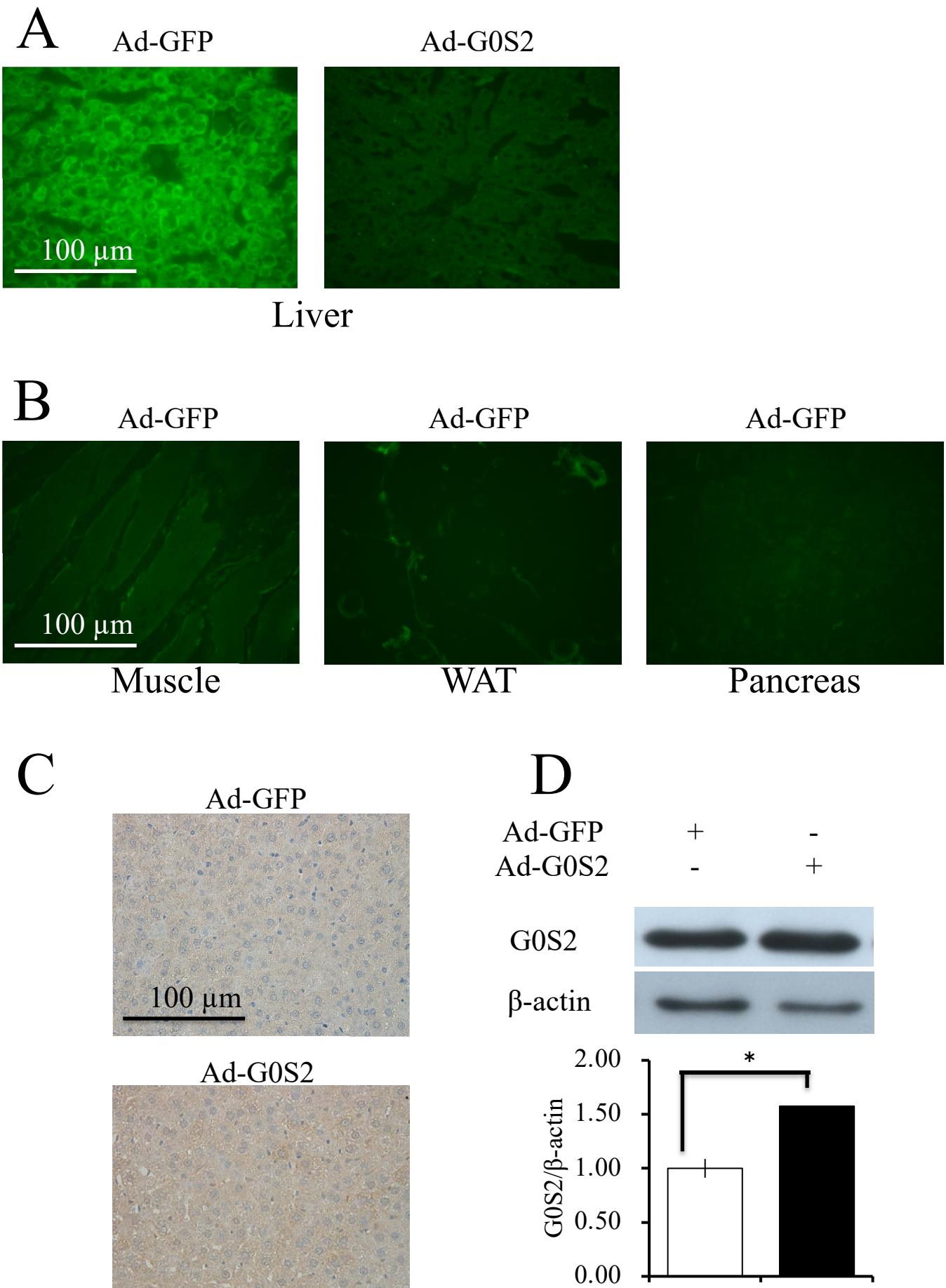
A
Ad-GFP
Ad-G0S2
100 μm
Liver
B
Ad-GFP
Ad-GFP
Ad-GFP
100 μm
Muscle
WAT
Pancreas
C
Ad-GFP
100 μm
Ad-G0S2
D
Ad-GFP + -
Ad-G0S2 - +
G0S2
β-actin
G0S2/β-actin
2.00
1.50
1.00
0.50
0.00
*

Figure 3.

A

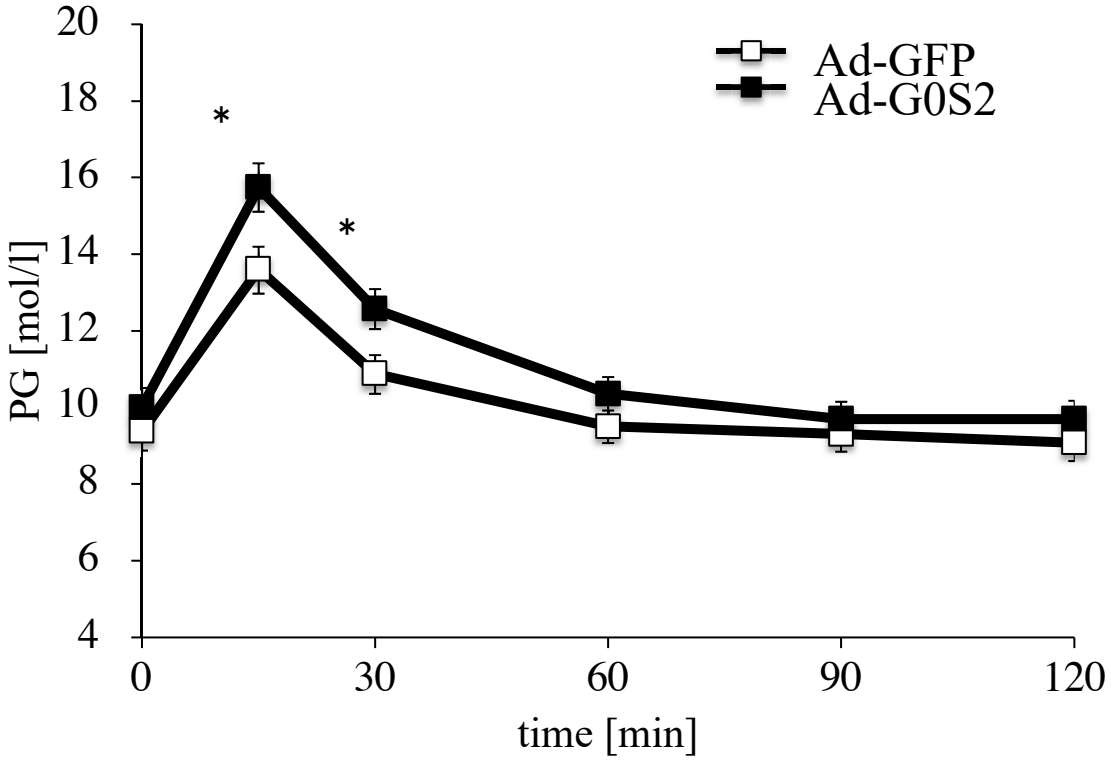
20
18
16
14
12
10
8
6
4
PG [mol/l]
*
*
Ad-GFP
Ad-G0S2
0
30
60
90
120
time [min]

B

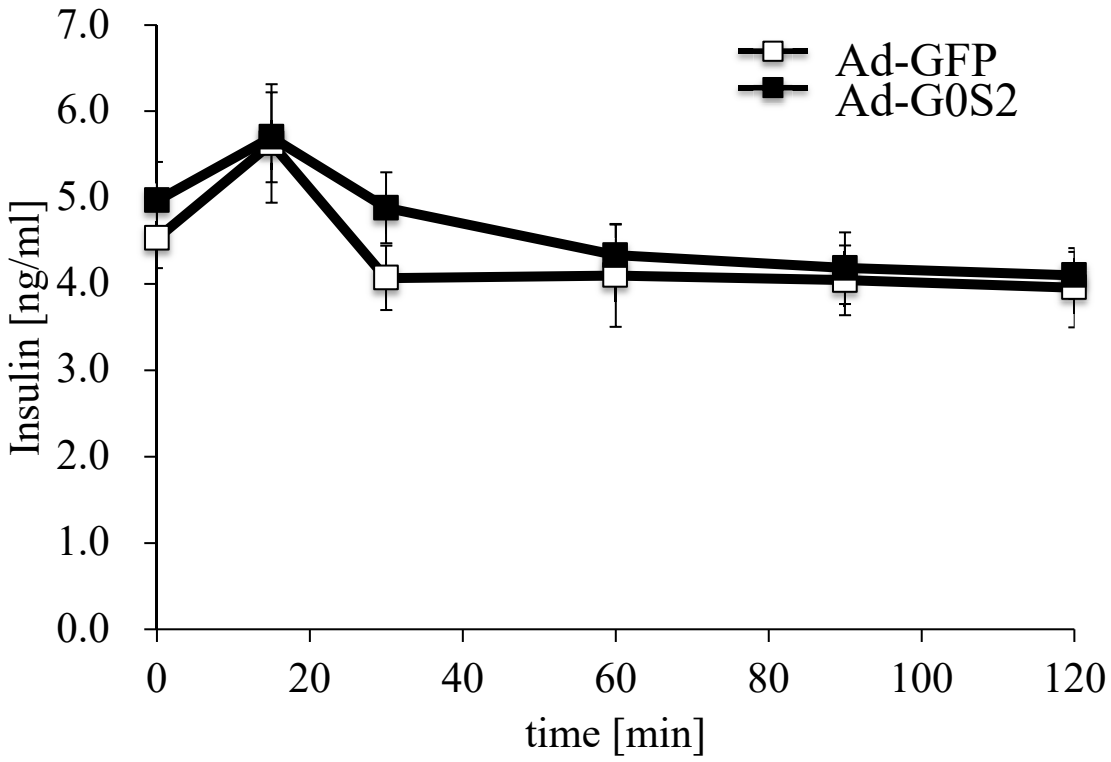
7.0
6.0
5.0
4.0
3.0
2.0
1.0
0.0
Insulin [ng/ml]
Ad-GFP
Ad-G0S2
0
20
40
60
80
100
120
time [min]

Figure 4.

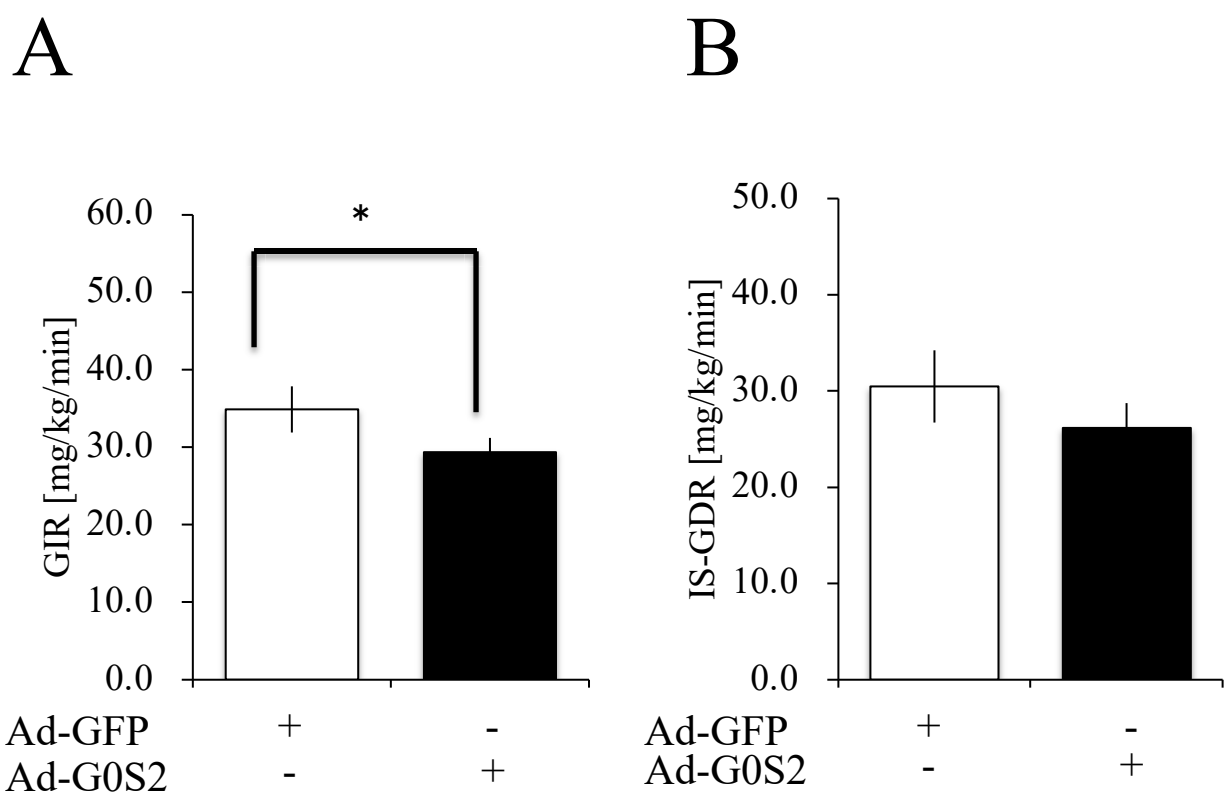
A
B
60.0
50.0
40.0
30.0
20.0
10.0
0.0
GIR [mg/kg/min]
*
50.0
40.0
30.0
20.0
10.0
0.0
IS-GDR [mg/kg/min]
Ad-GFP + -
Ad-G0S2 - +
Ad-GFP + -
Ad-G0S2 - +

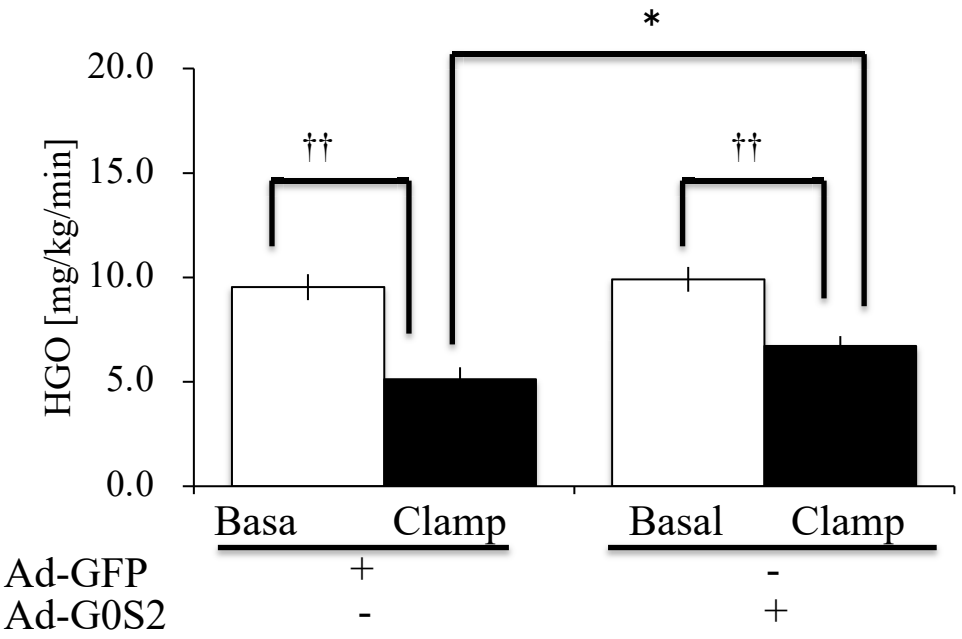
C
*
20.0
15.0
10.0
5.0
0.0
HGO [mg/kg/min]
††
††
Basa
Clamp
Basal
Clamp
Ad-GFP + -
Ad-G0S2 - +

Figure 5.

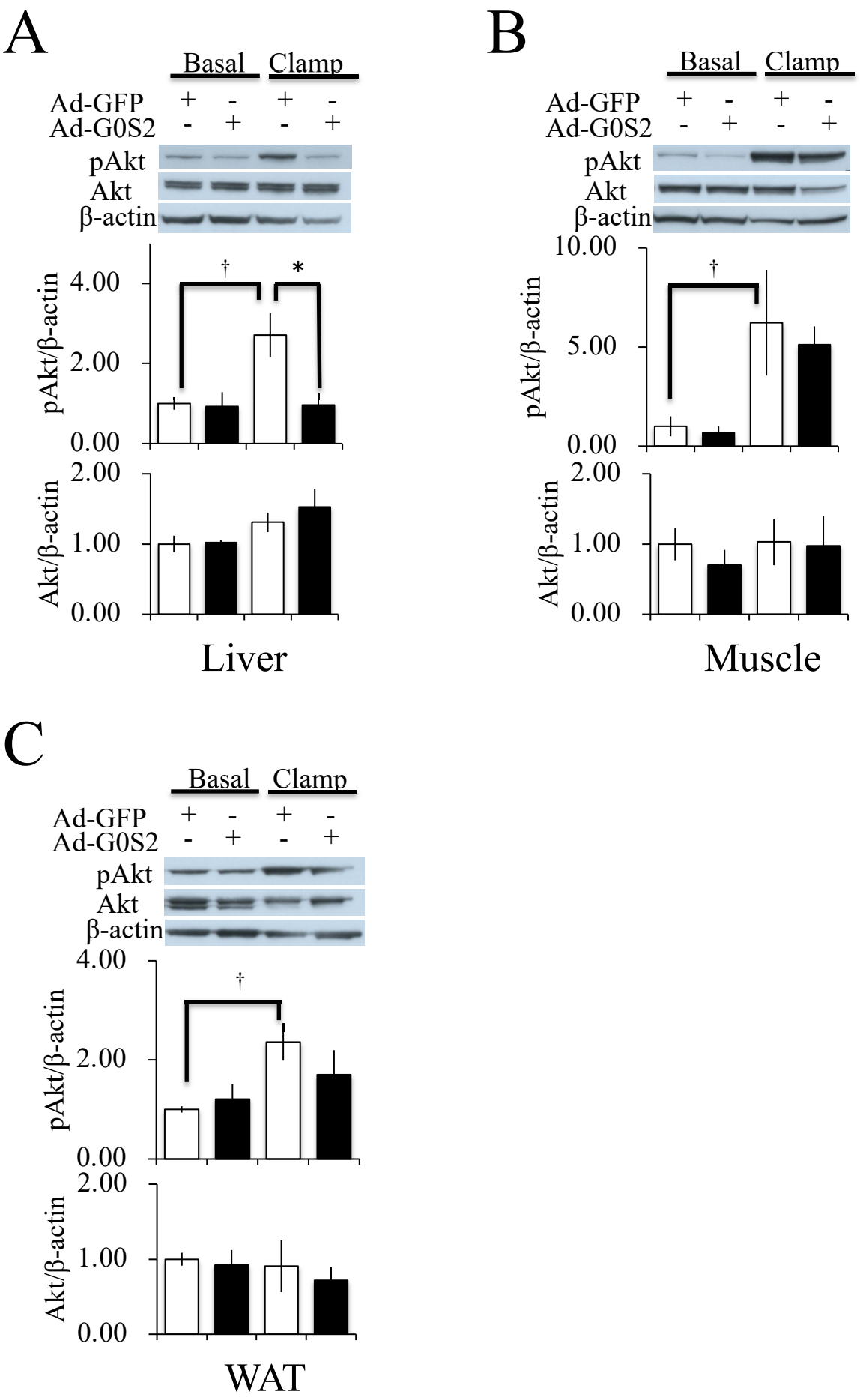
A
Basal
Clamp
Ad-GFP + - + -
Ad-G0S2 - + - +
pAkt
Akt
β-actin
pAkt/β-actin
4.00
2.00
0.00
†
*
Akt/β-actin
2.00
1.00
0.00
Liver
B
Basal
Clamp
Ad-GFP + - + -
Ad-G0S2 - + - +
pAkt
Akt
β-actin
pAkt/β-actin
10.00
5.00
0.00
†
Akt/β-actin
2.00
1.00
0.00
Muscle
C
Basal
Clamp
Ad-GFP + - + -
Ad-G0S2 - + - +
pAkt
Akt
β-actin
pAkt/β-actin
4.00
2.00
0.00
†
Akt/β-actin
2.00
1.00
0.00
WAT

Figure 6.

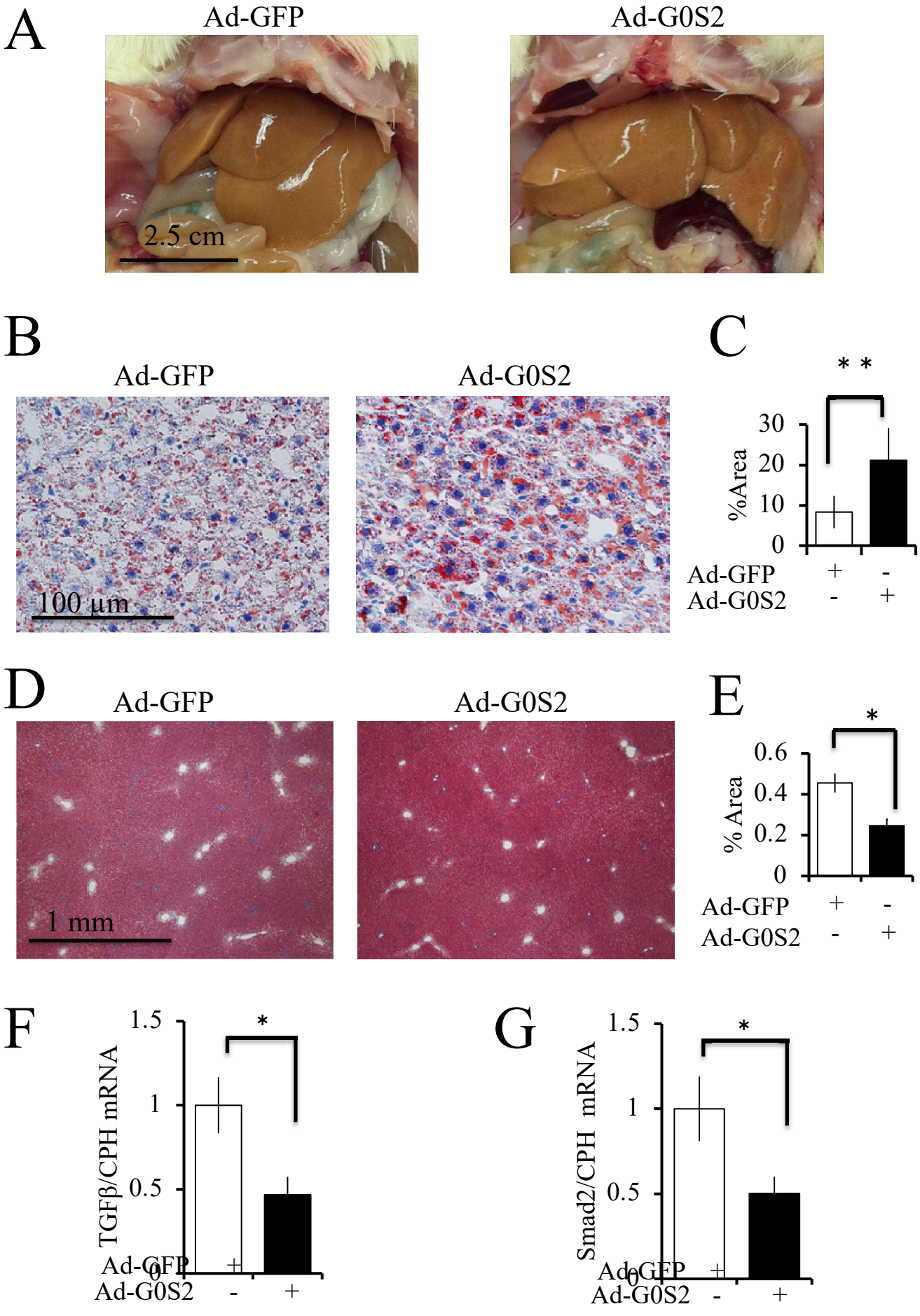
A
Ad-GFP
Ad-G0S2
2.5 cm
B
Ad-GFP
Ad-G0S2
100 μm
C
* *
%Area
30
20
10
0
Ad-GFP + -
Ad-G0S2 - +
D
Ad-GFP
Ad-G0S2
1 mm
E
*
% Area
0.6
0.4
0.2
0
Ad-GFP + -
Ad-G0S2 - +
F
*
TGFβ/CPH mRNA
1.5
1
0.5
0
Ad-GFP +
Ad-G0S2 - +
G
*
Smad2/CPH mRNA
1.5
1
0.5
0
Ad-GFP +
Ad-G0S2 - +